Journal of Materials Chemistry C

ROYAL SOCIETY OF CHEMISTRY

PAPER

View Article Online
View Journal

Cite this: DOI: 10.1039/d4tc00324a

The Hansen solubility approach towards green solvent processing: n-channel organic field-effect transistors under ambient conditions†

Ibrahim Deneme, Tevhide Ayça Yıldız, Nilgun Kayaci and Hakan Usta *

The adoption of green solvents is of utmost importance for the solution-based fabrication of semiconductor thin films and for the commercialization of (opto)electronic devices, especially in response to evolving regulatory mandates for handling organic materials. Despite the increasing interest in this area, the scarcity of green solvent-processed n-channel OFETs, especially functioning under ambient conditions, highlights the need for further research. In this study, we demonstrated the Hansen solubility approach to study the solubility behavior of an ambient-stable n-type semiconductor, 2,2′-(2,8-bis(3-dodecylthiophen-2-yl)indeno[1,2-*b*]fluorene-6,12-diylidene)dimalononitrile (**β,β′-C$_{12}$-TIFDMT**), and to analyze potential green solvents for thin-film processing. The Hansen solubility parameters were determined to be δ_D = 20.8 MPa$^{1/2}$, δ_P = 5.8 MPa$^{1/2}$, and δ_H = 5.5 MPa$^{1/2}$ with a radius (R_0) of 8.3 MPa$^{1/2}$. A green solvent screening analysis based on the minimal distance constraint and quantitative sustainability score identified ethoxybenzene, anisole, 2-methylanisole, and 2-methyltetrahydrofuran as suitable green solvents (R_a's = 5.17–7.93 MPa$^{1/2}$ < R_0). A strong thermodynamic correlation was identified between the solubility and the semiconductor–solvent distance in the 3D Hansen solubility space, in which the maximum solubility limit could be estimated with the enthalpy of fusion (ΔH_{fus}) and melting temperature (T_{mp}) of the semiconductor. To the best of our knowledge, this relationship between the maximum solubility limit and thermal properties has been established for the first time for organic semiconductors. Bottom-gate/top-contact OFETs fabricated by spin-coating the semiconductor green solutions exhibited μ_es reaching ~0.2 cm^2 V^{-1} s^{-1} (I_{on}/I_{off} ~10^6–10^7 and V_{on} ~0–5 V) under ambient conditions. This device performance, to our knowledge, is the highest reported for an ambient-stable green solvent-processed n-channel OFET. Our HSP-based rational approach and unique findings presented in this study can shed critical light on how green solvents can be efficiently incorporated in solution processing in organic (opto)electronics, and whether ambient-stable n-type semiconductors can continue to play an important role in green OFETs.

Received 22nd January 2024,
Accepted 17th February 2024

DOI: 10.1039/d4tc00324a

rsc.li/materials-c

Introduction

Electron-deficient π-conjugated small molecules represent a captivating class of organic materials that have shown tremendous potential as semiconductors in n-channel organic field-effect transistors (OFETs), as well as electron transport layers in a wide range of optoelectronic devices, including photovoltaics and light-emitting diodes/transistors.[1–4] Although a π-system functionalized with an electron-withdrawing group (*e.g.*, fluoro, imide, carbonyl, cyano, and dicyanovinylene) becomes technically π-electron-deficient,[5–7] the famous examples with high electron mobilities include naphthalene diimide,[8–10] perylene diimide,[11,12] quinoidal,[13–15] and indenofluorene[16,17] π-architectures. Small molecules offer a remarkable fine-tuning ability over frontier orbital energetics, optical transitions, physicochemical properties, and solubilities compared to polymers and macromolecules.[18–20] Furthermore, conventional synthesis and purification processes for small molecules enable the reproducible achievement of high purity levels with monodispersity and minimal batch-to-batch variations.[21–23] Over the past three decades, n-type semiconducting molecules have played an essential role in advancing the functions and performances of organic (opto)electronic devices, which has enabled a plethora of structural, physicochemical, mechanical, and optoelectronic properties that are mostly unattainable with conventional elemental or compound semiconductors.[5,24–26] Among these properties, solubility in organic solvents stands

Department of Nanotechnology Engineering, Abdullah Gül University, 38080 Kayseri, Turkey. E-mail: hakan.usta@agu.edu.tr

† Electronic supplementary information (ESI) available. See DOI: https://doi.org/10.1039/d4tc00324a

out as a unique tunable feature of molecular semiconductors that holds significant potential for large-scale roll-to-roll manufacturing.[25,27,28] Molecular semiconductors generally exhibit greater solubility in organic solvents compared to polymers, primarily due to the increased entropy of the mixing effect as dictated by statistical thermodynamics.[29,30] Despite these advantages, incorporating solubility into n-type semiconducting π-architectures, particularly in conjunction with ambient processing and ambient characterization of their corresponding semiconducting thin films, continues to present challenges from both molecular design and semiconductor device standpoints.[12,31,32] As a result, only a limited number of π-structures exhibiting these properties have been reported to date in OFETs.[8,9,14,15,33]

Solution-processable and ambient stable n-type semiconducting molecules have been mostly studied by processing their solutions in environmentally dangerous and toxic halogenated/aromatic hydrocarbon solvents such as chloroform, dichloromethane, chlorobenzene, and toluene.[5,8] These solvents not only pose significant risks to human health and diverse ecosystems but are also predominantly derived from fossil fuels, making them non-sustainable in nature.[29,34,35] In recent years, the utilization of green solvents in the solution processing of molecular semiconductors has emerged as a crucial research direction for advancing the future development of organic optoelectronics, yet with very limited examples for n-channel OFETs (Table S1, ESI†).[29,34,36,37] In one of these studies, Ho *et al.*[35] demonstrated green solvent-processed OFETs (μ_e = 0.07–0.13 $cm^2\ V^{-1}\ s^{-1}$ measured under vacuum) by shearing the solutions of n-type molecules *N*,*N*′-dioctyl-3,4,9,10-perylenedicarboximide and *N*,*N*′-bis(*n*-alkyl)-(1,7 and 1,6)-dicyanoperylene-3,4 : 9,10-bis(dicarboximide) (**PTCDI-C8** and **PDIF-CN2**, respectively, in Table S1, ESI†) in anisole and Purasolv EHL (2-ethylhexyl ester of natural L-lactic acid). In another study, Harris *et al.*[38] reported the synthesis of a bay-functionalized PDI-based molecular semiconductor (**X1** in Table S1, ESI†), which exhibited μ_es of $\sim 5 \times 10^{-5}$ $cm^2\ V^{-1}\ s^{-1}$ (measured under vacuum) in their green solvent (alcohol/amine binary mixture) processed thin films in n-channel OFETs. In a very recent study by Corzo *et al.*,[39] an electron-deficient molecule (**O-IDTBR** in Table S1, ESI†), which is typically used as an acceptor in bulk-heterojunction solar cells, was processed from a terpene biosolvent into an n-type semiconducting film in bottom-contact/top-gate OFETs (μ_e ~0.37–0.91 $cm^2\ V^{-1}\ s^{-1}$ as measured under vacuum). Alternatively, the utilization of green solvents as non-solvent additives to modify the morphology and crystallinity of the semiconductor has also been demonstrated, rather than relying solely on the dissolving capabilities of pure green solvents.[40,41] In another recent study by Wang *et al.*,[42] a versatile high-resolution patterning strategy was developed for the fabrication of ultraflexible transistor circuitry, which demonstrated a semiconducting channel (μ_e ~0.1 $cm^2\ V^{-1}\ s^{-1}$) based on the n-semiconducting polymer, N2200, processed from an environmentally benign solvent, THF, under ambient conditions. In a recent study by Lee *et al.*,[43] binary semiconductor solution systems were prepared by introducing 2-methyltetrahydrofuran (2-MeTHF) into the chloroform solution of an n-type polymer (**P(NDI2OD-T2)** in Table S1, ESI†), and diethyl succinate into the chlorobenzene solution of an n-type small molecule (**TU-3** in Table S1, ESI†). This approach led to n-channel OFETs with μ_es ranging from 0.13 to 0.33 $cm^2\ V^{-1}\ s^{-1}$, as measured under vacuum conditions.

Despite the recent efforts, the obtainment of green solvent processed n-channel OFETs with favorable electron mobilities ($\mu_e > 0.1\ cm^2\ V^{-1}\ s^{-1}$) and transistor characteristics ($I_{on}/I_{off} \geq 10^5$ and $V_{on} \sim 0$ V) measured under ambient conditions remains highly challenging, emphasizing the need for further studies. At this point, it is important to highlight that during solution processing, specific solute–solvent interactions, along with solvent properties such as evaporation rate, viscosity/surface wettability, and film-forming capacity, critically influence the molecular self-assembly process.[2,8,45,46] Altering the solvent used for the semiconductor can result in notable changes in the microstructural and morphological characteristics of thin films, subsequently impacting the efficiency of electron transport. Hence, replacing toxic and non-sustainable solvents with environmentally friendly and sustainable alternatives is not a straightforward effort, and it requires a rational approach. Due to the intricate nature of solubility involving a wide range of interaction types, it is essential to conduct rational studies, rather than a trial-and-error approach, in order to determine which green solvents are compatible with a specific semiconductor. For this purpose, utilizing solubility parameters (δs) proves to be a practical approach. This concept was first introduced by Hildebrand and Scott in the 1950s,[47,48] which is defined as the square root of the total cohesive energy density ($\delta = (E_{cohesive}/V_{molar})^{1/2}$), and was later extended by Hansen[47,49] in 1967 to include three distinct interaction contributions of dispersive (δ_D), polar (δ_P), and hydrogen-bonding (δ_H) origins, which are defined as Hansen solubility parameters (HSPs). A fundamental understanding of this theory posits that the total cohesive energy of a molecule comprises three primary intermolecular forces: dispersion, polarity, and hydrogen bonding, and molecules can only dissolve each other if they possess similar specific interaction strengths. In a similar manner, this principle can be extended to organic semiconductors, with each semiconductor anticipated to show a specific δ_D, δ_P, and δ_H coordinate point in the 3D Hansen solubility space. Additionally, a solubility sphere, determined by an interaction radius (R_0), can be defined based on the specific solubility criteria relevant to a given application.[22,50,51]

In this study, by employing a HSP analysis-aided rational solubility approach, we explore potential green solvents for the ambient-stable, high-performance n-type semiconducting molecule, **β,β′-C_{12}-TIFDMT** (Fig. 1). This semiconductor, synthesized in-house at a half-gram scale, was chosen for this study due to its excellent n-channel behavior (μ_e ~0.9 $cm^2\ V^{-1}\ s^{-1}$, I_{on}/I_{off} ~10^7–10^8, and V_{on} ~0 V under ambient conditions) in bottom-gate/top-contact OFETs, when processed from chlorinated solvents.[52] The solubility of the semiconductor across a set of 30 organic solvents with diverse chemical structures and HSPs were determined by UV-Vis absorption spectroscopy and gravimetric methods. The solubilities ranged from 7.3 g L^{-1}

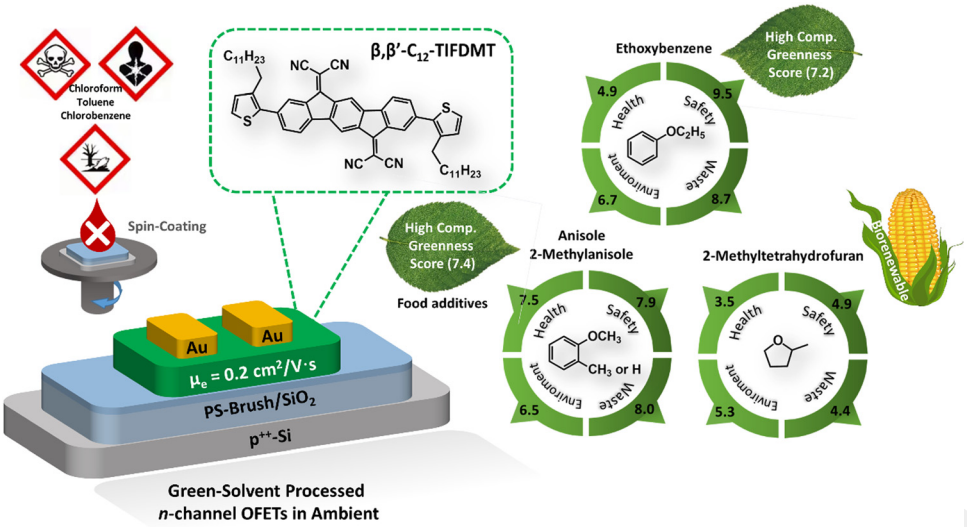

Fig. 1 A bottom-gate/top-contact OFET device structure (p^{++}-Si/SiO_2/PS-brush/semiconductor/Au) was employed in this study to study green solvents, and the chemical structure of the ambient-stable n-type semiconductor, 2,2′-(2,8-bis(3-dodecylthiophen-2-yl)indeno[1,2-*b*]fluorene-6,12-diylidene)dimalononitrile (**β,β′-C_{12}-TIFDMT**). The chemical structures of the green solvents, anisole, 2-methylanisole, ethoxybenzene, and 2-methyltetrahydrofuran, are shown with the corresponding GlaxoSmithKline (GSK)'s[44] four category scores of health, safety, environment, and waste (disposal). Representative hazard pictograms based on the "globally harmonized system of classification and labelling of chemicals" (GHS) are also shown for some toxic and environmentally hazardous solvents (*e.g.*, chloroform, toluene, and chlorobenzene).

(8.3×10^{-3} M) to 0.03 g L^{-1} (3.0×10^{-5} M) and insolubility, and the HSPs were determined to be δ_D = 20.8 $MPa^{1/2}$, δ_P = 5.8 $MPa^{1/2}$, and δ_H = 5.5 $MPa^{1/2}$ with a radius (R_0) of 8.3 $MPa^{1/2}$ based on the solubility sphere method using classic Hansen algorithm in HSPiP software.[53] A green solvent screening analysis was then performed by using the minimal distance constraint ($R_a < R_0$) and the solvent sustainability credits. Accordingly, ethoxybenzene (R_a = 5.19 $MPa^{1/2}$), anisole (R_a = 6.32 $MPa^{1/2}$), 2-methylanisole (R_a = 5.17 $MPa^{1/2}$), and 2-methyltetrahydrofuran (R_a = 7.93 $MPa^{1/2}$) were identified as suitable green solvents for solution processing, all of which yield sufficient solubilities ($\geq$4 g L^{-1}) for thin-film processing. In addition, a strong thermodynamic correlation was identified between the solubility and the semiconductor–solvent distance in the 3D Hansen solubility space, from which the maximum solubility limit could be estimated with the semiconductor's thermal properties of melting enthalpy (ΔH_{fusion}) and temperature (T_m). Bottom-gate/top-contact OFETs were fabricated under ambient conditions by spin-coating the semiconductor green solutions onto p^{++}-Si/SiO_2/PS-brush (M_n = 5 kDa) substrates. Clear n-channel transistor behaviors were observed under ambient conditions with μ_es reaching ~0.2 cm^2 V^{-1} s^{-1}, I_{on}/I_{off} ~ 10^6–10^7, and V_{on} ~0–5 V.

Experimental section

Materials and methods

All reagents and solvents were obtained from commercial vendors and used as received, unless otherwise noted. **β,β′-C_{12}-TIFDMT** was synthesized in accordance with the synthesis and purification methods outlined in our previous report.[52] Differential scanning calorimetry (DSC) was performed under nitrogen at a heating rate of 10 C min^{-1} on a Mettler Toledo DSC822e instrument. Indium and zinc standards (Mettler Toledo, Schwerzenbach, Switzerland) were used for calibration in DSC. UV-Vis absorption spectra were recorded on a Shimadzu UV-1800 UV-Vis spectrophotometer. Hansen solubility sphere, parameters, and fitting accuracy were determined by using the classic Hansen algorithm in the HSPiP Program (*5th Edition Version 5.4.08*) with a solubility limit of 2 g L^{-1}.[53] Solubility scores of "1" and "0" are assigned for good and bad solvents, respectively. The group contribution methodology was employed using neural network techniques in the HSPiP program.

Solubility measurements

The semiconductor solubility in various solvents was measured by UV-Vis absorption spectroscopy. First, a linear calibration curve was generated at the semiconductor's absorption maximum (λ_{max} = 338 nm) in chloroform by collecting the UV-Vis absorption spectra of standard solutions (4.55×10^{-7}–4.55×10^{-5} M). Then, saturated semiconductor solutions were prepared by weighing a small amount (~5.0 mg) of the organic semiconductor solid into a vial and adding 500 μL of a particular solvent *via* a micropipette. Next, the mixture was stirred/sonicated for 30 min at room temperature, filtered through a PTFE syringe filter (VWR, part of Avantor, 0.20 μm pore size), and diluted (200×) with chloroform in order to reach an optical absorption region in the range of the calibration curve. For each solvent, the absorbance at the absorption maximum was measured, and the corresponding solubility value was calculated by substituting this absorbance value into the calibration curve equation based on the Beer–Lambert law ($A = \varepsilon \cdot b \cdot c$). When the solubility exceeds 1.0 g L^{-1} in a particular solvent, an additional gravimetric method is also used for

confirmation. In the gravimetric method, a small amount (~5.0 mg) of the semiconductor solid was precisely weighed into a vial, and incremental volumes (in 50–100 μL portions) of a particular solvent were added *via* a micropipette. After each addition, the solution was stirred/sonicated for 10 min at room temperature. Solvent addition was continued until complete dissolution was visually observed. Once complete dissolution was confirmed, the semiconductor solution was filtered through a PTFE syringe filter (VWR, part of Avantor, 0.20 μm pore size) and then evaporated to dryness with a rotary evaporator. The gravimetric solubility was calculated based on the recovered semiconductor solid weight (m_{osc}) and the total amount of solvent ($V_{solvent}$) using the following equation: solubility = $m_{osc}/V_{solvent}$.

OFET device fabrication and characterization

β,β′-C$_{12}$-TIFDMT thin films (~40–45 nm) were deposited onto the PS-brush-treated substrates, p^{++}-Si/SiO$_2$/PS-brush (M_n = 5 kDa), by spin-coating the corresponding semiconductor solutions in anisole, 2-methylanisole, ethoxybenzene, and 2-methyltetrahydrofuran (4.0 mg mL^{-1}) at 1500, 1700, and 2000 rpm under ambient conditions. The thin films were thermally annealed at 170, 190 and 200 °C (for 30 min) in a vacuum oven. The bottom-gate/top-contact OFET devices were finished by thermal evaporation of Au source–drain electrodes (50 nm thick, growth rate of 0.2 Å s^{-1}). Semiconducting channels with lengths (L) and widths (W) of 30/40/50/60/80 μm and 1000 μm, respectively, were obtained. The transistor characteristics were measured using a Keithley 2614B source-measure unit in an Everbeing BD-6 probe station under ambient conditions (without excluding natural or fluorescent lighting). Electron mobilities (μ_e), threshold voltages (V_T), and I_{on}/I_{off} ratios were calculated in the saturation regime by the following formula:

$$\mu_{sat} = \left(\frac{2L}{W \times C_{ox}}\right)\frac{I_{DS}}{(V_G - V_T)^2}$$

where I_{DS} is the source–drain current, L is the channel length, W is the channel width, C_{ox} is the areal capacitance of the gate dielectric with the PS-brush interlayer per unit area (taken as 10.5 nF cm^{-2}),[54] V_G is the gate voltage, and V_T is the threshold voltage. The reported values are the averages of at least ten different devices. The surface morphologies and microstructures of the semiconductor thin films were investigated by atomic force microscopy on a NanoSurf FlexAFM C3000 instrument and grazing incidence X-ray diffraction (GIXRD) on a Malvern Panalytical Empyrean diffractometer.

Results and discussion

Study of solubility and determination of Hansen solubility parameters

The n-type semiconductor, **β,β′-C$_{12}$-TIFDMT**, was synthesized in-house at a half-gram scale, following the synthesis and purification methods outlined in our previous report.[52] In order to determine the semiconductor HSP sphere and the corresponding parameters, we employed a set of 30 organic solvents (Table 1) encompassing diverse structures, including aromatics, alcohols, polar aprotic solvents, non-polar solvents, chlorinated alkanes/aromatics, terpenes, and esters. These solvents exhibited a wide range of δ_D (14.5–20.0), δ_P (0–18.0), and δ_H (0–26.0) values in the Hansen space to improve the fitting of the semiconductor solubility sphere. The maximum solubility of these solvents was measured by using UV-Vis absorption spectroscopy. The initial step involved generating a linear calibration curve at maximum molecular absorption (Fig. S1, ESI†). A molar absorptivity value (ε) of 5.85 × 10^4 M^{-1} cm^{-1} was obtained by fitting the calibration curve (Fig. 2(a)) using the Beer–Lambert law. The saturated semiconductor solutions were prepared in 30 different solvents and were diluted with chloroform in order to reach an optical absorption region in the range of the calibration curve shown in Fig. 2(a). Here, it is important to note that the diluted semiconductor solutions showed the same spectra in the 325–450 nm region as the original spectrum recorded in pure chloroform (Fig. 2(b)). This is a result of the presence of a residual test solvent in the diluted solutions (0.5% (v/v)), which highlights the method's ability to give accurate maximum absorbance values. For each solvent, absorbance at λ_{max} = 338 nm was measured and translated into the corresponding solubility value by using a calibration curve equation. On the other hand, for the solvents with a solubility ≥ 1.0 g L^{-1}, an additional gravimetric method was also employed for confirmation, which yielded solubility results within ~3–4% of the spectroscopic method.

As shown in Table 1, **β,β′-C$_{12}$-TIFDMT** exhibited a broad spectrum of solubilities in 30 different organic solvents, ranging from complete insolubility to as high as 7.3 g L^{-1} (8.3 × 10^{-3} M), with variation dependent on the specific solute–solvent interactions. In particular, chlorinated alkanes/aromatics (4.9–7.3 g L^{-1} (5.6–8.3 × 10^{-3} M): chloroform, methylene dichloride, and chlorobenzene) and aromatics (2.0–6.7 g L^{-1} (2.3–7.6 × 10^{-3} M): benzene, toluene, *o*-xylene) were found to be the best solvents for **β,β′-C$_{12}$-TIFDMT**. Also, a good solubility value of 5.3 g L^{-1} (6.0 × 10^{-3} M) was recorded in tetrahydrofuran. 1-Butanol, cyclopentanone, 1,4-dioxane, methyl iso-butyl ketone, *N*-methyl-2-pyrrolidone, *N,N*-dimethylformamide *n*-amyl acetate, ethyl acetate, and *d*-limonene showed solubilities in the range of 0.13–1.11 g L^{-1} (0.15–1.26 × 10^{-3} M). Solubility in the remaining solvents was ≤0.10 g L^{-1}. The solubility scores of "1" (indicating a good solvent) and "0" (indicating a non-solvent) were assigned based on a threshold concentration value of 2.0 g L^{-1} at room temperature. Under the assumption of a spherical solubility sphere, the best fitting accuracy (0.999) was attained using the classic Hansen algorithm in the HSPiP program (Fig. S2, ESI†).[53] As shown in Fig. 2(c), the HSPs for **β,β′-C$_{12}$-TIFDMT** were determined to be δ_D = 20.8 MPa$^{1/2}$, δ_P = 5.8 MPa$^{1/2}$, and δ_H = 5.5 MPa$^{1/2}$ with an interaction radius (R_0) of 8.3 MPa$^{1/2}$. Given that $\delta_D \gg \delta_P$ and δ_H, the major source of cohesive energy in the solid state ($E_{cohesive}$) for **β,β′-C$_{12}$-TIFDMT** arises from dispersion interactions, with polar and hydrogen-bonding contributions playing comparatively lesser roles. While Hansen's original solubility theory does not explicitly address π-interactions, the dispersion term (δ_D)

Table 1 The solubility values (both in g L^{-1} and M) of **β,β′-C_{12}-TIFDMT** in 30 different organic solvents determined *via* the spectroscopic (UV-Vis absorption) method, the corresponding Hansen solubility parameters (δ_D, δ_P, δ_H in $MPa^{1/2}$), and the specific semiconductor–solvent interaction distance ($R_a = (4\Delta\delta_D^2 + \Delta\delta_P^2 + \Delta\delta_H^2)^{1/2}$ in $MPa^{1/2}$, in which $\Delta\delta$ for a specific Hansen parameter is "$\delta_{OSC}-\delta_{solvent}$"). The solubility scores "1" (for a good solvent) and "0" (for a non-solvent) are given based on the threshold concentration value of 2.0 g L^{-1}

Solvent	Hansen parameters ($MPa^{1/2}$)			Solubility (g L^{-1})	Molarity ($\times10^{-3}$ M)	Interaction distance (R_a) ($MPa^{1/2}$)	Solubility score
	δ_D	δ_P	δ_H				
Aromatics							
Benzene	18.4	0	2.0	2.01	2.29	8.3	1
Toluene	18.0	1.4	2.0	6.70	7.60	7.9	1
o-Xylene	17.8	1.0	3.1	5.02	5.71	8.0	1
Alcohols							
1-Butanol	16.0	5.7	15.8	0.10	0.11	14.1	0
tert-Butanol	15.2	5.1	14.7	0.03	0.03	14.5	0
Ethanol	15.8	8.8	19.4	Insoluble	—	—	0
Ethylene glycol	17.0	11.0	26.0	Insoluble	—	—	0
Methanol	14.7	12.3	22.3	0.03	0.03	21.8	0
2-Propanol	15.8	6.1	16.4	Insoluble	—	—	0
Polar aprotic							
Acetone	15.5	10.4	7.0	0.05	0.06	11.7	0
Acetonitrile	15.3	18.0	6.1	Insoluble	—	—	0
Cyclopentanone	17.9	11.9	5.2	0.79	0.90	8.4	0
Diethyl ether	14.5	2.9	4.6	0.04	0.05	13.0	0
Dimethyl sulfoxide	18.4	16.4	10.2	Insoluble	—	—	0
N,*N*-Dimethylformamide	17.4	13.7	11.3	0.13	0.15	11.9	0
1,4-Dioxane	17.5	1.8	9	1.11	1.26	8.5	0
Ethylene carbonate	18.0	21.7	5.1	Insoluble	—	—	0
Methyl iso-butyl ketone	15.3	6.1	4.1	0.14	0.16	11.1	0
N-Methyl-2-pyrrolidone	18.0	12.3	7.2	0.50	0.57	8.7	0
Propylene carbonate	20.0	18.0	4.1	0.05	0.06	12.4	0
Tetrahydrofuran	16.8	5.7	8.0	5.30	6.00	8.4	1
Chlorinated alkanes/aromatics							
Chloroform	17.8	3.1	5.7	6.92	7.81	6.6	1
Methylene dichloride	17.0	7.3	7.1	4.93	5.62	7.9	1
Chlorobenzene	19.0	4.3	2.0	7.30	8.30	5.2	1
Esters							
n-Amyl acetate	15.8	3.3	6.1	0.16	0.18	10.3	0
Ethyl acetate	15.8	5.3	7.2	0.13	0.15	10.2	0
Propylene glycol monoethyl ether acetate	15.6	6.3	7.7	0.08	0.09	10.6	0
Terpenes							
d-Limonene	17.2	1.8	4.3	0.30	0.34	8.3	0
Non-polar							
Cyclohexane	16.8	0	0.2	0.08	0.09	11.2	0
Hexane	14.9	0	0	0.05	0.06	14.3	0

obtained herein indeed comprises π-interactions (*i.e.*, π···π, C–H···π, and N/S···π) between the relatively large, rod-shaped and polarizable **TIFDMT** donor–acceptor–donor π-backbones, as well as dispersion interactions between aliphatic dodecyl substituents.[55,56] Note that while the strength of the latter interactions is important for thin-film crystallization and microstructure, the former interactions are essential in establishing an electronic structure for efficient charge transport.[52,57] The major contribution of the dispersion interactions in the **β,β′-C_{12}-TIFDMT**'s HSP parameters was also evident with the group contribution methodology (Fig. S3, ESI†). This approach was employed in the HSPiP using neural network techniques,[58,59] in which the **β,β′-C_{12}-TIFDMT** molecular structure is divided into various aromatic-aliphatics-functional group components and the HSPs are estimated as the sum of the contributions from these components. On the basis of the solubility parameters, the best solvents, chlorobenzene (7.3 g L^{-1}) and chloroform (6.9 g L^{-1}), are calculated to give the closest interaction distances to **β,β′-C_{12}-TIFDMT** (R_a = 5.2 $MPa^{1/2}$ and 6.6 $MPa^{1/2}$, respectively) compared to all other solvents. This serves as an additional validation of the precision and reliability of our HSP analysis for the present semiconductor. Given that the δ_D value of our semiconductor is 20.8 $MPa^{1/2}$, solvents with greater solubilities generally have δ_D values exceeding ~17–18 $MPa^{1/2}$. This is primarily because the difference in the dispersion parameters ($\Delta\delta_D$s) has a fourfold effect on the R_a calculation, in contrast to the effects of polar ($\Delta\delta_P$) or hydrogen bonding ($\Delta\delta_H$) parameters.[47,50] Conversely, when considering the moderate δ_P and δ_H values of **β,β′-C_{12}-TIFDMT** (5.5–5.8 $MPa^{1/2}$), solvents with extremely high or low δ_P and δ_H values (*i.e.*, very polar and non-polar solvents) tend to result in very low solubility. These observations lay the groundwork for a fundamental understanding of the upcoming green solvent analysis.

Quantitative correlation of the semiconductor solubility and HSP parameters

A key advantage of HSP analysis is the ability to establish a quantitative thermodynamic correlation between solubility values and the interaction distances (R_as) in the 3D Hansen space for semiconductors. Surprisingly, this still largely remains unexplored in the field of (opto)electronics. Despite

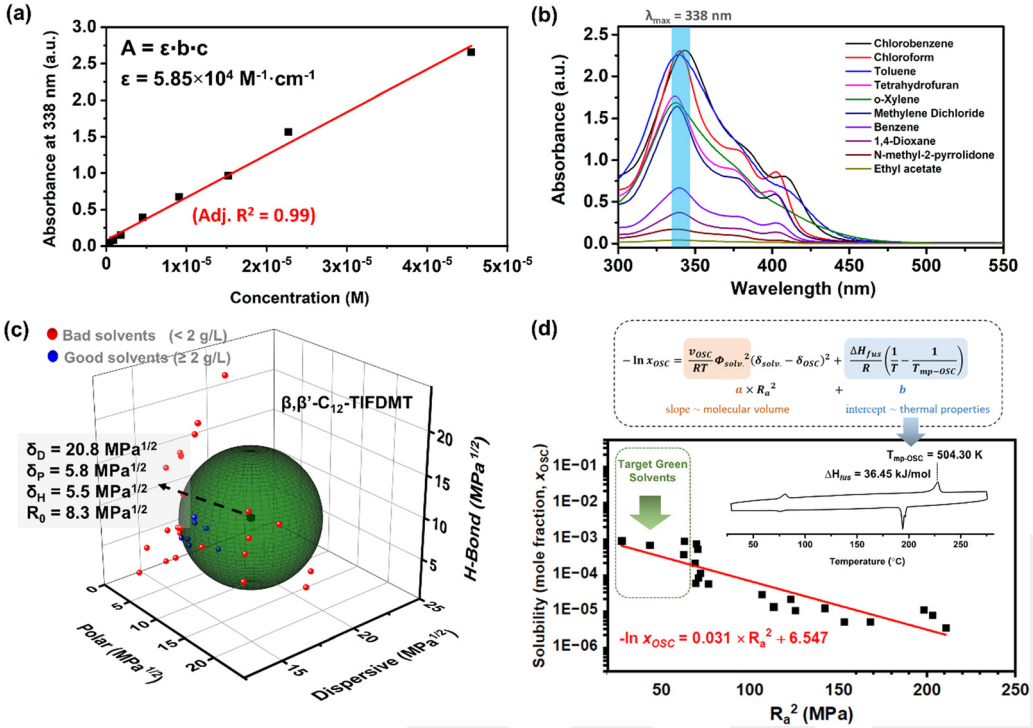

Fig. 2 (a) The calibration curve based on the absorbance of **β,β′-C$_{12}$-TIFDMT** in chloroform at varied standard solution concentrations (4.55×10^{-7} M–4.55×10^{-5} M) recorded at absorption maximum (λ_{max} = 338 nm); the linear fitting was performed according to Beer–Lambert law (adjusted R^2 is 0.99). (b) Optical absorption spectra of **β,β′-C$_{12}$-TIFDMT** in saturated solutions in selected organic solvents after 200× dilution with chloroform. (c) Hansen solubility sphere and parameters of **β,β′-C$_{12}$-TIFDMT** were determined by using the classic Hansen algorithm (HSPiP Program) with a solubility limit of 2 g L^{-1}. The Hansen solubility parameters (δ_D, δ_P, δ_H, and R_0) are in MPa$^{1/2}$, and the bad (23) and the good (7) solvents are shown in the 3D Hansen solubility space with red and blue spheres, respectively. (d) The linear correlation between the semiconductor solubility in the mole fraction unit (x_{OSC}) and the squared solute–solvent distance (R_a^2) in the HSP space (correlation coefficient ~ −0.9), and the logarithmic equation derived based on the Scatchard–Hildebrand regular solution theory.[50] Inset shows the differential scanning calorimetry (10 °C min^{-1} heating ramp under N_2) scan of **β,β′-C$_{12}$-TIFDMT** with the corresponding enthalpy of fusion (ΔH_{fus}) and the melting temperature ($T_{mp\text{-}OSC}$) values.

several studies exploring the HSPs of semiconductors,[22,39,44] to the best of our knowledge, such a correlation has been examined in only a few previous reports, and a direct relationship with thermal characteristics has not been established.[50,60,61] As the solubilities of our semiconductor ranged over almost three orders of magnitude among 24 solvents, and these solvents gave widely ranged semiconductor–solvent interaction distances (R_a) of 5.2–21.8 MPa$^{1/2}$ (Table 1) in the 3D Hansen space, we were able to study such thermodynamic correlations for **β,β′-C$_{12}$-TIFDMT**. Note that these six solvents are omitted from this analysis since the semiconductor is practically insoluble in these solvents. This correlation was based on a Hansen-adapted Scatchard–Hildebrand regular solution theory,[50,62] in which the squared difference in the Hildebrand solubility parameters $(\delta_1 - \delta_2)^2$ is replaced by the squared interaction distance (R_a^2) in the HSP space. As shown in eqn (1), R is the gas constant and T is the solubility measurement temperature (absolute). A logarithmic relationship between the R_a^2 value and the solubility mole fraction (x_{OSC}) would be expected if the Hansen solubility parameters for the semiconductor were accurately determined.

$$-\ln x_{OSC} = \frac{v_{OSC}}{RT}\Phi_{solv.}{}^2 R_a{}^2 + \frac{\Delta H_{fus}}{R}\left(\frac{1}{T} - \frac{1}{T_{mp\text{-}OSC}}\right) \quad (1)$$

In this equation, the slope depends on the molar volume (v_{OSC}) of the subcooled liquid of the pure semiconductor solid and the solvent volume fraction ($\Phi_{solv.} \approx 1$ for dilute solutions), the intercept is a function of the thermal properties of the semiconductor solid, which are the semiconductor's enthalpy of fusion (ΔH_{fus}) and the melting temperature ($T_{mp\text{-}OSC}$). The slope indicates the sensitivity of the semiconductor solubility to changes in the R_a value, while the intercept represents the maximum solubility limit of the semiconductor in an ideal solvent as R_a approaches 0. The second part of eqn (1) indeed shows the solubility equation described for ideal solutions.[63] Additionally, it is important to note that in eqn (1), the Flory–Huggins correction term for the entropy of mixing is considered to be significantly smaller than the HSP term, and as a result, it is not included in the calculation.[61] As shown in Fig. 2(d), when x_{OSC} is plotted against R_a^2 on a logarithmic scale (see Table S2 for data details, ESI†), a strong negative correlation (correlation coefficient ≈ -0.9) was calculated between these two parameters and the relationship can be regressed to the equation given in Fig. 2(d). Most importantly, the intercept is calculated to be 6.547, and it matches very well with the enthalpy of fusion (ΔH_{fus} = 36.45 kJ mol^{-1}) and the melting temperature ($T_{mp\text{-}OSC}$ = 504.30 K) of the semiconductor

solid obtained *via* differential scanning calorimetry (DSC) (Fig. S4, see the ESI† for details). This correspondence between the Scatchard–Hildebrand regular solution theory and DSC characteristics is highly promising and has the potential to pave the way for a new approach in semiconductors, enabling the prediction of their maximum solubility limits solely based on thermal characteristics.

Exploring suitable green solvents for semiconductor processing

In light of the recent regulatory demands concerning chemical substances, the adoption of green solvent processing is undeniably important for solution-based fabrication of organic (opto)electronic devices.[39,44,64] The qualification of an organic liquid as a green solvent is a multifaceted concept that reflects diverse and sometimes controversial aspects of health, safety, environmental impact, and overall sustainability. More specifically, the solvents could be evaluated and classified into ten distinct subcategories: health hazard, exposure potential, flammability and explosion, reactivity and stability, air impact, aqueous impact, incineration, recycling, biotreatment, and volatile organic compounds, according to the regularly updated GlaxoSmithKline (GSK) solvent sustainability guide.[65,66] As demonstrated by Larsen *et al.* in a quantitative methodology,[44] these subcategories could be converted into four category scores and then combined to generate a composite score value (G). The G value ranges between 1 and 10, and a high score (>7) is desirable for a solvent suggesting a favorable greenness. On the other hand, the green solvent of choice should be able to dissolve the semiconductor at the required concentrations, which is at least 4.0 mg mL^{-1} at room temperature or moderately elevated temperatures ($\sim$50–60 °C) in our case for spin-coating. According to the Hansen solubility approach,[22,47,49] the selection of a green solvent to dissolve a semiconducting molecule strictly depends on the similarities between the dispersive, polar, and hydrogen-bonding interactions (*i.e.*, δ_D, δ_P, and δ_H values, respectively) of the pure green solvent and the semiconductor structure. In other words, the similarities between these interactions lead to a reduction in the interaction distance (R_a), thereby increasing molecular solubility.

On the basis of the HSPs determined for **β,β′-C_{12}-TIFDMT** (δ_D = 20.8 $MPa^{1/2}$, δ_P = 5.8 $MPa^{1/2}$, and δ_H = 5.5 $MPa^{1/2}$), a set of potential green solvents (21 green solvents shown in Table S3, ESI†) were screened by using the minimal distance constraint ($R_a < R_0$ = 8.3 $MPa^{1/2}$) in the 3D Hansen solubility space and sustainability credits. Consequently, we identified four solvents with reasonably small interaction distances: ethoxybenzene (R_a = 5.19 $MPa^{1/2}$), anisole (R_a = 6.32 $MPa^{1/2}$), 2-methylanisole (R_a = 5.17 $MPa^{1/2}$), and 2-methyltetrahydrofuran (R_a = 7.93 $MPa^{1/2}$). Here, it is noteworthy that these R_a values are expected to align with the high solubility region of the Scatchard–Hildebrand fitting curve in Fig. 2(d), aiming to achieve solubilities exceeding 10^{-3} M, which is sufficient for thin-film fabrication. These solvents exhibit relatively larger δ_D values (16.9–18.4 $MPa^{1/2}$) compared to other environmentally friendly solvents, which, as previously mentioned, highlights the significant role of dispersion interactions in determining the overall solubility. Moreover, the boiling points of these solvents are in a reasonable temperature range (boiling points $\approx$ 78–170 °C), which is crucial for an effective spin-coating process to achieve favorable semiconducting morphologies and microstructures.[29,67,68] With regard to the greenness of these solvents, anisole and 2-methylanisole are well-known food additives,[29,37,69] while ethoxybenzene and anisole exhibit excellent sustainability with high G values of 7.2 and 7.4, respectively.[44] In this context, it is worth highlighting that the GSK composite score for ethoxybenzene might potentially be even higher, as a relatively conservative health score (4.9) was assigned to ethoxybenzene due to limited information available in this particular category.[44] In today's industry, although anisole production predominantly relies on petrochemicals, we note that it is also

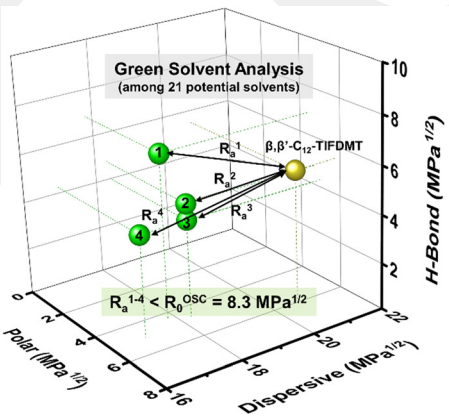

#	Solvent (CAS Number)	δ_D	δ_P	δ_H	R_a	GSK Greenness Scores/GHS of Classification-Labelling of Chemicals
1	Anisole (100-66-3)	17.8	4.4	6.9	6.3	Health = 7.5 Safety = 7.9 Environment = 6.5 Waste = 8.0 Composite Score = 7.4 H226, H315, H319, H336
2	2-Methylanisole (578-58-5)	18.3	4.7	4.8	5.2	Certified Food Additive H226, H302
3	Ethoxybenzene (103-73-1)	18.4	4.5	4	5.2	Health = 4.9 Safety = 9.5 Environment = 6.7 Waste = 8.7 Composite Score = 7.2 H226
4	2-Methyltetrahydrofuran (96-47-9)	16.9	5	4.3	7.9	Health = 3.5 Safety = 4.9 Environment = 5.3 Waste = 4.4 Composite Score = 4.4 H225, H302, H315, H318, H319, H335, H336 Biorenewable

Fig. 3 Hansen solubility parameters (δ_D, δ_P, δ_H in $MPa^{1/2}$) of four potential green solvents, anisole (1), 2-methylanisole (2), ethoxybenzene (3), and 2-methyltetrahydrofuran (4), and their corresponding semiconductor–solvent interaction distances with respect to **β,β′-C_{12}-TIFDMT** (R_a^{1-4} = $(4\Delta\delta_D^2 + \Delta\delta_P^2 + \Delta\delta_H^2)^{1/2}$ in $MPa^{1/2}$, in which $\Delta\delta$ for a specific Hansen parameter is "$\delta_{OSC} - \delta_{solvent}$"). The GlaxoSmithKline (GSK)'s four category scores of health, safety, environment, and waste (disposal) are shown in the table for the green solvents, along with the composite scores and the representative hazard statements based on the "globally harmonized system of classification and labelling of chemicals" (GHS),[44] in which H225: highly flammable liquid and vapor, H226: flammable liquid and vapor, H302: harmful if swallowed, H315: causes skin irritation, H318: serious eye damage, H319: serious eye irritation, H335: may cause respiratory irritation, H336: may cause drowsiness or dizziness.

possible to obtain anisole from renewable sources such as lignin and guaiacol.[70] On the other hand, despite its relatively lower greenness compared to our other three green solvents, 2-methyltetrahydrofuran is a biorenewable green solvent and it could be manufactured with a carbon footprint of ~40× reduced CO_2 emission as compared to conventional tetrahydrofuran.[71]

Thin-film microstructure/morphology and field-effect transistor characterization

After determining four potential green solvents for our n-type semiconductor processing, bottom-gate/top-contact OFETs were fabricated by spin coating **β,β′-C$_{12}$-TIFDMT** green solutions (4.0 g L^{-1}) in anisole, 2-methylanisole, ethoxybenzene, and 2-methyltetrahydrofuran onto p^{++}-Si/SiO_2/PS-brush (M_n = 5 kDa) substrates. An ultrathin (~3.6 nm) polystyrene brush (PS-brush) layer was employed since its densely packed (grafting density ≈ 0.45 chains nm^{-2}) hydrophobic surface facilitates the formation of a proper microstructure for efficient electron transport.[52,54] When selecting these green solvents, the similarity of the dispersive, polar, and hydrogen-bonding interactions between the semiconductor and the solvents serves not only to enhance molecular solubility but also to promote uninterrupted molecular arrangement during solution processing. This is because it reduces the likelihood of abrupt and drastic changes in the short-range intermolecular cohesive forces when transitioning from a solution state, where semiconducting molecules are surrounded by solvent molecules, to a thin-film state, where semiconducting molecules interact only with each other. This phenomenon has indeed been evident in the literature, where a majority of the high-performing semiconducting thin films were fabricated from solvents with favorable solubility parameters (*e.g.*, chloroform, toluene, and

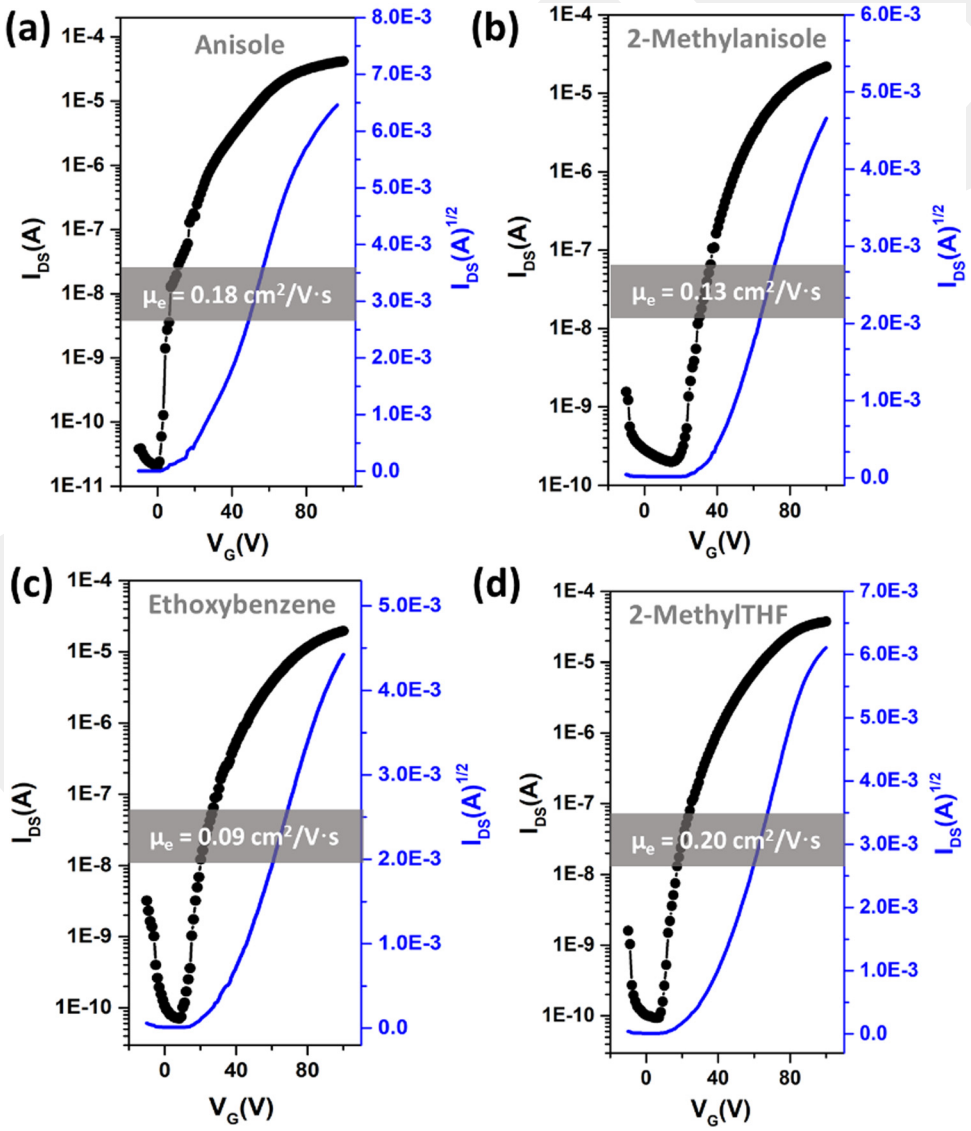

Fig. 4 Transfer plots (V_{DS} = 100 V) for the fabricated OFET devices of **β,β′-C$_{12}$-TIFDMT** on p^{++}-Si/SiO_2/PS-brush (M_n = 5 kDa) spin-coated from anisole (a), 2-methylanisole (b), ethoxybenzene (c), and 2-methyltetrahydrofuran (d) solutions. All measurements were performed under ambient conditions, and the electron mobilities were based on the transfer curves shown herein.

chlorobenzene), despite the absence of Hansen solubility parameter (HSP) analyses in most of these studies.[5,46,72]

In order to completely realize the potential of these green solvents to yield favorable microstructures with efficient electron transport, spin-coating rates of 1500, 1700, and 2000 rpm were used and the semiconductor thin films were thermally annealed at temperatures of 170 °C, 190 °C, and 200 °C. Typical transfer and output plots are shown in Fig. 4 and Fig. S5 (ESI†), and the transistor results for all these conditions are listed in Table S4 (ESI†). The OFETs from all four solvents exhibited clear n-channel characteristics under ambient conditions. In their best working conditions, the OFETs processed from anisole and 2-methyltetrahydrofuran gave μ_{max} = 0.18–0.20 cm^2 V^{-1} s^{-1} (μ_{avg} = 0.07–0.13 ± 0.04) with I_{on}/I_{off} ratios of ∼10^6–10^7 and threshold voltages (V_Ts) of 2.1–9.4 V, while the OFETs from 2-methylanisole and ethoxybenzene yielded μ_{max} = 0.09–0.13 cm^2 V^{-1} s^{-1} (μ_{avg} = 0.05 ± 0.03) with I_{on}/I_{off} ratios of ∼10^5–10^6 and slightly increased V_Ts of 18.4–27.1 V. In particular, in the transfer curve of the thin film fabricated from anisole (Fig. 4(a)), a clear near-zero turn-on voltage is evident. The hysteresis of the I_{DS}–V_G transfer characteristics was also analyzed for all the green solvents, and a lower back-sweep current hysteresis behavior was observed for all OFETs with ΔV_G magnitudes ($\Delta V_G = V_G^R - V_G^F$ at I_{DS} of ∼10^{-7}–10^{-8} A) of 8–19 V (Fig. S6, ESI†). A similar behavior with relatively larger hysteresis magnitudes was observed in recently reported green-solvent-processed OFETs.[35] This could potentially be attributed to charge carrier trapping in deep states and electronic effects at the dielectric–semiconductor interface.[73,74] As shown in Fig. 5, thin films processed from anisole, 2-methylanisole, and ethoxybenzene exhibited two-dimensional micron-sized (∼1–3 μm) grains that are grown in the substrate plane. However, their microstructures did not reveal a large crystallinity in the out-of-plane direction, showing weak (100) peaks in the low-angle region (2θ = 3.35–3.46°) and broad (010) peaks in the higher-angle (2θ = 21.20–21.40°) region. On the other hand, thin films processed from 2-methyltetrahydrofuran exhibit a different morphology with smaller grains (∼400–600 nm). In the 2-methyltetrahydrofuran-processed thin films, long-range ordering in the out-of-plane direction was evident with a strong (100) peak at 2θ = 3.43° along with the presence of (200) and (300) diffraction peaks. Based on the observed broad (010) peaks, we note that short-range π-interactions (∼4.1 Å) were present for all thin films. Among the four green solvents employed in thin-film fabrication, thin films processed from 2-methyltetrahydrofuran yields the highest crystallinity with a strong out-of-plane long-range ordering. Considering that the solution concentration and the dielectric surface are the same for all four green solvents, the observed greater crystallization performance of **β,β′-C$_{12}$-TIFDMT** from 2-methyltetrahydrofuran suggests a different solvent–solute interaction behavior in 2-methyltetrahydrofuran, compared with the other green solvents. We analyzed the R_a^2 values for all the green solvents (R_a^{1-4} in Fig. 3) in order to explore the solvent–semiconductor interaction differences. The larger the value of R_a^2, the larger the differences in the cohesive energetics of the semiconductor and solvent, and the lower the semiconductor solubility in that particular solvent based on the Hansen-adapted Scatchard–Hildebrand regular solution theory, as discussed earlier. Amazingly, 2-methyltetrahydrofuran exhibits the largest R_a^2 value (62.41) compared to those of the other green solvents (R_a^2 = 27–39.69 for anisole, 2-methylanisole, and ethoxybenzene) (Fig. 3). Based on our HSP analysis, the large R_a^2 value likely contributes to the strong molecular self-assembly behavior observed in 2-methyltetrahydrofuran during spin coating as the solvent evaporates, leading to thin-film crystallization.

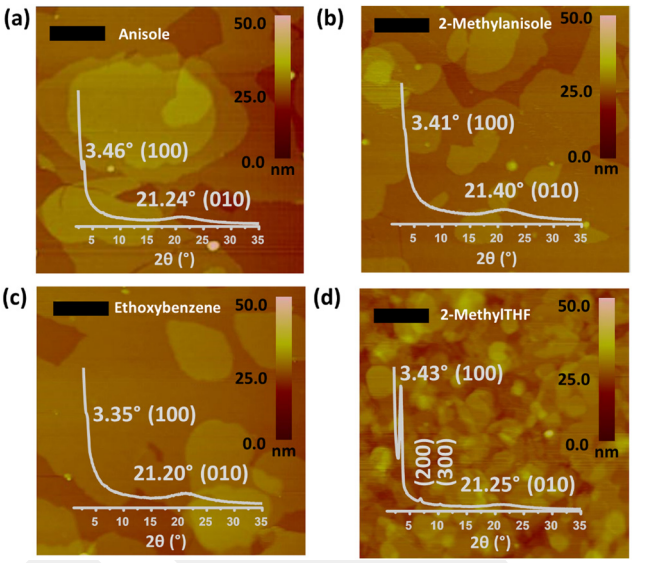

Fig. 5 Spin-coated thin films of **β,β′-C$_{12}$-TIFDMT** on a p^{++}-Si/SiO$_2$/PS-brush (M_n = 5 kDa) from anisole (a), 2-methylanisole (b), ethoxybenzene (c), and 2-methyltetrahydrofuran (d) solutions. Top-view atomic force microscopy (AFM) topography images and the corresponding out-of-plane grazing-incidence X-ray diffraction (GIXRD) patterns (insets) with 2θ diffraction angles and assigned crystallographic planes. Scale bars denote 1 μm. The annealing temperature for each device is 170–190 °C.

Conclusions

In summary, the solubility behavior of an ambient-stable n-type semiconductor, 2,2′-(2,8-bis(3-dodecylthiophen-2-yl)indeno[1,2-*b*]-fluorene-6,12-diylidene)dimalononitrile (**β,β′-C$_{12}$-TIFDMT**), was studied using the solubility sphere method and classic Hansen algorithm. As the solubility in 30 different solvents ranged from 7.3 g L^{-1} (8.3 × 10^{-3} M) to 0.03 g L^{-1} (3.0 × 10^{-5} M) and insolubility, the HSPs were determined to be δ_D = 20.8 MPa$^{1/2}$, δ_P = 5.8 MPa$^{1/2}$, and δ_H = 5.5 MPa$^{1/2}$ with an interaction radius (R_0) of 8.3 MPa$^{1/2}$. A strong thermodynamic correlation based on the Scatchard–Hildebrand regular solution theory was identified between the molecular solubility and the semiconductor–solvent interaction distance R_a. From the fitting curve, it is evident that the maximum solubility limit could be estimated from the semiconductor's thermal properties of the enthalpy of fusion (ΔH_{fus}) and melting temperature (T_{mp}). To the best of our knowledge, this relationship has been established for the first time for organic semiconductors. Using the minimal distance constraint in the HSP

space and quantitative sustainability score, four suitable green solvents (*i.e.*, ethoxybenzene, anisole, 2-methylanisole, and 2-methyltetrahydrofuran) were identified for **β,β′-C_{12}-TIFDMT** with R_as of 5.17–7.93 $MPa^{1/2}$ ($<R_0$). These solvents yielded sufficient solubility ($\geq$ 4 g L^{-1}) for thin-film processing. Bottom-gate/top-contact OFETs were fabricated by spin-coating the semiconductor green solutions, and the μ_e values reached $\sim$0.2 cm^2 V^{-1} s^{-1} (I_{on}/I_{off} $\sim 10^6$–10^7 and V_{on} $\sim$0–5 V) under ambient conditions. To our knowledge, this n-channel device performance is the highest reported for ambient-stable green solvent-processed OFET. Our HSP-based rational approach, an emerging yet underexplored methodology in the field, along with the unique findings presented herein, has the potential to significantly contribute to the integration of green solvents into the solution processing of n-channel semiconductors and to the broader development of charge-transport materials for green optoelectronics.

Author contributions

H. U. conceived and designed the experiments. I. D. synthesized and purified the small molecular semiconductor. T. A. Y. and I. D. fabricated and characterized the organic field-effect transistors. N. K. performed the solubility measurements. H. U. wrote the paper. All authors discussed the results and commented on the manuscript.

Conflicts of interest

There are no conflicts to declare.

Acknowledgements

H. U., I. D., T. A. Y., and N. K. acknowledge support from the Scientific and Technological Research Council of Turkey (TUBITAK) (grant no. 121C261). We thank Prof. Gokhan Demirel and Prof. Fahri Alkan for fruitful discussions.

References

1 C. Lee, S. Lee, G.-U. Kim, W. Lee and B. J. Kim, *Chem. Rev.*, 2019, **119**, 8028–8086.
2 O. Ostroverkhova, *Chem. Rev.*, 2016, **116**, 13279–13412.
3 X. Gao and Y. Hu, *J. Mater. Chem. C*, 2014, **2**, 3099–3117.
4 S. Moschetto, E. Benvenuti, H. Usta, R. Ozdemir, A. Facchetti, M. Muccini, M. Prosa and S. Toffanin, *Adv. Mater. Interfaces*, 2022, **9**, 2101926.
5 H. Usta, A. Facchetti and T. J. Marks, *Acc. Chem. Res.*, 2011, **44**, 501–510.
6 A. Riaño, P. Mayorga Burrezo, M. J. Mancheño, A. Timalsina, J. Smith, A. Facchetti, T. J. Marks, J. T. López Navarrete, J. L. Segura, J. Casado and R. Ponce Ortiz, *J. Mater. Chem. C*, 2014, **2**, 6376.
7 Y. Wang, H. Guo, S. Ling, I. Arrechea-Marcos, Y. Wang, J. T. López Navarrete, R. P. Ortiz and X. Guo, *Angew. Chem., Int. Ed.*, 2017, **56**, 9924–9929.
8 F. Zhang, Y. Hu, T. Schuettfort, C. Di, X. Gao, C. R. McNeill, L. Thomsen, S. C. B. Mannsfeld, W. Yuan, H. Sirringhaus and D. Zhu, *J. Am. Chem. Soc.*, 2013, **135**, 2338–2349.
9 Y. Hu, Y. Qin, X. Gao, F. Zhang, C. A. Di, Z. Zhao, H. Li and D. Zhu, *Org. Lett.*, 2012, **14**, 292–295.
10 B. A. Jones, A. Facchetti, T. J. Marks and M. R. Wasielewski, *Chem. Mater.*, 2007, **19**, 2703–2705.
11 J. Zhang, L. Tan, W. Jiang, W. Hu and Z. Wang, *J. Mater. Chem. C*, 2013, **1**, 3200–3206.
12 B. A. Jones, M. J. Ahrens, M.-H. Yoon, A. Facchetti, T. J. Marks and M. R. Wasielewski, *Angew. Chem.*, 2004, **116**, 6523–6526.
13 C. Zhang, Y. Zang, E. Gann, C. R. McNeill, X. Zhu, C. A. Di and D. Zhu, *J. Am. Chem. Soc.*, 2014, **136**, 16176–16184.
14 Q. Wu, R. Li, W. Hong, H. Li, X. Gao and D. Zhu, *Chem. Mater.*, 2011, **23**, 3138–3140.
15 A. Velusamy, C. Yu, S. N. Afraj, C. Lin, W. Lo, C. Yeh, Y. Wu, H. Hsieh, J. Chen, G. Lee, S. Tung, C. Liu, M. Chen and A. Facchetti, *Adv. Sci.*, 2021, **8**, 2002930.
16 H. Usta, C. Risko, Z. Wang, H. Huang, M. K. Deliomeroglu, A. Zhukhovitskiy, A. Facchetti and T. J. Marks, *J. Am. Chem. Soc.*, 2009, **131**, 5586–5608.
17 A. Can, A. Facchetti and H. Usta, *J. Mater. Chem. C*, 2022, **10**, 8496–8535.
18 K. Takimiya, S. Shinamura, I. Osaka and E. Miyazaki, *Adv. Mater.*, 2011, **23**, 4347–4370.
19 M. M. Torrent and C. Rovira, *Chem. Soc. Rev.*, 2008, **37**, 827–838.
20 S. Ma, J. Wang, K. Feng, H. Zhang, Z. Wu, Y. Wang, B. Liu, Y. Li, M. An, R. Gonzalez-Nuñez, R. Ponce Ortiz, H. Y. Woo and X. Guo, *ACS Appl. Mater. Interfaces*, 2023, **15**, 1639–1651.
21 H. Usta and A. Facchetti, *Large Area and Flexible Electronics*, Wiley-VCH Verlag GmbH & Co. KGaA, Weinheim, Germany, 2015, pp. 1–100.
22 I. Burgués-Ceballos, F. Machui, J. Min, T. Ameri, M. M. Voigt, Y. N. Luponosov, S. A. Ponomarenko, P. D. Lacharmoise, M. Campoy-Quiles and C. J. Brabec, *Adv. Funct. Mater.*, 2014, **24**, 1449–1457.
23 G.-S. Ryu, Z. Chen, H. Usta, Y.-Y. Noh and A. Facchetti, *MRS Commun.*, 2016, **6**, 47–60.
24 B. J. Jung, N. J. Tremblay, M.-L. Yeh and H. E. Katz, *Chem. Mater.*, 2011, **23**, 568–582.
25 S. E. Root, S. Savagatrup, A. D. Printz, D. Rodriquez and D. J. Lipomi, *Chem. Rev.*, 2017, **117**, 6467–6499.
26 M. N. Le, K. Baeg, K. Kim, S. Kang, B. D. Choi, C. Park, S. Jeon, S. Lee, J. Jo, S. Kim, J. Park, D. Ho, J. Hong, M. Kim, H. Kim, C. Kim, K. Kim, Y. Kim, S. K. Park and M. Kim, *Adv. Funct. Mater.*, 2021, **31**, 2103285.
27 T. Kim, J.-H. Kim, T. E. Kang, C. Lee, H. Kang, M. Shin, C. Wang, B. Ma, U. Jeong, T.-S. Kim and B. J. Kim, *Nat. Commun.*, 2015, **6**, 8547.
28 H. Zhu, E. Shin, A. Liu, D. Ji, Y. Xu and Y. Noh, *Adv. Funct. Mater.*, 2020, **30**, 1904588.
29 J. Lee, S. A. Park, S. U. Ryu, D. Chung, T. Park and S. Y. Son, *J. Mater. Chem. A*, 2020, **8**, 21455–21473.

30 J. Lee, C. Sun, B. S. Ma, H. J. Kim, C. Wang, J. M. Ryu, C. Lim, T. Kim, Y. Kim, S. Kwon and B. J. Kim, *Adv. Energy Mater.*, 2021, **11**, 2003367.
31 H. Usta, A. Facchetti and T. J. Marks, *J. Am. Chem. Soc.*, 2008, **130**, 8580–8581.
32 R. Ozdemir, D. Choi, M. Ozdemir, H. Kim, S. T. Kostakoğlu, M. Erkartal, H. Kim, C. Kim and H. Usta, *ChemPhysChem*, 2017, **18**, 850–861.
33 L. Wang, J. S. Park, H. G. Lee, G.-U. Kim, D. Kim, C. Kim, S. Lee, F. S. Kim and B. J. Kim, *ACS Appl. Mater. Interfaces*, 2020, **12**, 56240–56250.
34 F. Campana, C. Kim, A. Marrocchi and L. Vaccaro, *J. Mater. Chem. C*, 2020, **8**, 15027–15047.
35 D. Ho, J. Lee, S. Park, Y. Park, K. Cho, F. Campana, D. Lanari, A. Facchetti, S. Seo, C. Kim, A. Marrocchi and L. Vaccaro, *J. Mater. Chem. C*, 2020, **8**, 5786–5794.
36 T. L. Nguyen, C. Lee, H. Kim, Y. Kim, W. Lee, J. H. Oh, B. J. Kim and H. Y. Woo, *Macromolecules*, 2017, **50**, 4415–4424.
37 S. Pang, Z. Chen, J. Li, Y. Chen, Z. Liu, H. Wu, C. Duan, F. Huang and Y. Cao, *Mater. Horiz.*, 2023, **10**, 473–482.
38 D. H. Harris, S. Brixi, B. S. Gelfand, B. H. Lessard and G. C. Welch, *J. Mater. Chem. C*, 2020, **8**, 9811–9815.
39 D. Corzo, D. Rosas-Villalva, A. C, G. Tostado-Blázquez, E. B. Alexandre, L. H. Hernandez, J. Han, H. Xu, M. Babics, S. De Wolf and D. Baran, *Nat. Energy*, 2023, **8**, 62–73.
40 H. Opoku, B. Nketia-Yawson, E. S. Shin and Y.-Y. Noh, *Org. Electron.*, 2017, **41**, 198–204.
41 H. Opoku, B. Nketia-Yawson, E.-S. Shin and Y.-Y. Noh, *J. Mater. Chem. C*, 2018, **6**, 661–667.
42 B. Wang, W. Huang, S. Lee, L. Huang, Z. Wang, Y. Chen, Z. Chen, L.-W. Feng, G. Wang, T. Yokota, T. Someya, T. J. Marks and A. Facchetti, *Nat. Commun.*, 2021, **12**, 4937.
43 Y. Lee, D. Ho, F. Valentini, T. Earmme, A. Marrocchi, L. Vaccaro and C. Kim, *J. Mater. Chem. C*, 2021, **9**, 16506–16515.
44 C. Larsen, P. Lundberg, S. Tang, J. Ràfols-Ribé, A. Sandström, E. Mattias Lindh, J. Wang and L. Edman, *Nat. Commun.*, 2021, **12**, 4510.
45 J. Rivnay, S. C. B. Mannsfeld, C. E. Miller, A. Salleo and M. F. Toney, *Chem. Rev.*, 2012, **112**, 5488–5519.
46 C. Wang, H. Dong, W. Hu, Y. Liu and D. Zhu, *Chem. Rev.*, 2012, **112**, 2208–2267.
47 A. F. M. Barton, *Chem. Rev.*, 1975, **75**, 731–753.
48 J. H. Hildebrand, *Chem. Rev.*, 1949, **44**, 37–45.
49 C. M. Hansen, *Hansen solubility parameters: A user's handbook*, 2nd edn, 2007.
50 Y. Takebayashi, N. Morii, K. Sue, T. Furuya, S. Yoda, D. Ikemizu and H. Taka, *Ind. Eng. Chem. Res.*, 2015, **54**, 8801–8808.
51 F. Machui, S. Langner, X. Zhu, S. Abbott and C. J. Brabec, *Sol. Energy Mater. Sol. Cells*, 2012, **100**, 138–146.
52 A. Can, I. Deneme, G. Demirel and H. Usta, *ACS Appl. Mater. Interfaces*, 2023, **15**, 41666–41679.
53 S. Abbott and Y. Hiroshi, *Hansen Solubility Parameters Pract. Version 5.4.08*, Copyr. © 2008/23 Prof. Steven Abbott Dr Yamamoto Hiroshi (accessed August 2023).
54 S. H. Park, H. S. Lee, J.-D. Kim, D. W. Breiby, E. Kim, Y. D. Park, D. Y. Ryu, D. R. Lee and J. H. Cho, *J. Mater. Chem.*, 2011, **21**, 15580–15586.
55 E. M. Pérez and N. Martín, *Chem. Soc. Rev.*, 2015, **44**, 6425–6433.
56 J. P. Wagner and P. R. Schreiner, *Angew. Chem., Int. Ed.*, 2015, **54**, 12274–12296.
57 R. Ozdemir, S. Park, İ. Deneme, Y. Park, Y. Zorlu, H. A. Alidagi, K. Harmandar, C. Kim and H. Usta, *Org. Chem. Front.*, 2018, **5**, 2912–2924.
58 A. Randová and L. Bartovská, *Fluid Phase Equilib.*, 2016, **429**, 166–176.
59 E. Stefanis and C. Panayiotou, *Int. J. Thermophys.*, 2008, **29**, 568–585.
60 X.-Z. Shao, L.-S. Wang and M.-Y. Li, *Ind. Eng. Chem. Res.*, 2012, **51**, 5082–5089.
61 Y. Takebayashi, K. Sue, T. Furuya and S. Yoda, *J. Chem. Eng. Data*, 2018, **63**, 3889–3901.
62 G. Scatchard, *Chem. Rev.*, 1931, **8**, 321–333.
63 P. W. Atkins and J. De Paula, *Atkins' Physical Chemistry*, *8th edn*, Oxford University Press, London, England, 2006.
64 F. P. Byrne, S. Jin, G. Paggiola, T. H. M. Petchey, J. H. Clark, T. J. Farmer, A. J. Hunt, C. Robert McElroy and J. Sherwood, *Sustainable Chem. Processes*, 2016, **4**, 7.
65 R. K. Henderson, C. Jiménez-González, D. J. C. Constable, S. R. Alston, G. G. A. Inglis, G. Fisher, J. Sherwood, S. P. Binks and A. D. Curzons, *Green Chem.*, 2011, **13**, 854.
66 C. M. Alder, J. D. Hayler, R. K. Henderson, A. M. Redman, L. Shukla, L. E. Shuster and H. F. Sneddon, *Green Chem.*, 2016, **18**, 3879–3890.
67 D. Chen, A. Nakahara, D. Wei, D. Nordlund and T. P. Russell, *Nano Lett.*, 2011, **11**, 561–567.
68 H. Lee, C. Park, D. H. Sin, J. H. Park and K. Cho, *Adv. Mater.*, 2018, **30**, 1–39.
69 J. Lee, M. Malekshahi Byranvand, G. Kang, S. Y. Son, S. Song, G.-W. Kim and T. Park, *J. Am. Chem. Soc.*, 2017, **139**, 12175–12181.
70 F. G. Delolo, E. N. dos Santos and E. V. Gusevskaya, *Green Chem.*, 2019, **21**, 1091–1098.
71 C. S. Slater, M. J. Savelski, D. Hitchcock and E. J. Cavanagh, *J. Environ. Sci. Health, Part A: Toxic/Hazard. Subst. Environ. Eng.*, 2016, **51**, 487–494.
72 H. Dong, X. Fu, J. Liu, Z. Wang and W. Hu, *Adv. Mater.*, 2013, **25**, 6158–6183.
73 M.-H. Yoon, C. Kim, A. Facchetti and T. J. Marks, *J. Am. Chem. Soc.*, 2006, **128**, 12851–12869.
74 M. Egginger, S. Bauer, R. Schwödiauer, H. Neugebauer and N. S. Sariciftci, *Monatsh. Chem.*, 2009, **140**, 735–750.